2014

Accounting for Local Thermal Distortions in a Chamber Model for Twin Screw Compressors

David Buckney
Howden Compressors Ltd., United Kingdom, david.buckney@howden.com

Ahmed Kovacevic
City University London, Centre for Positive Displacement Compressor Technology, London, UK, a.kovacevic@city.ac.uk

Nikola Stosic
City University London, Centre for Positive Displacement Compressor Technology, London, UK, n.stosic@city.ac.uk

Accounting for Local Thermal Distortions in a Chamber Model for Twin Screw Compressors

David BUCKNEY[12]*, Ahmed KOVACEVIC[21], Nikola STOSIC[2]

[1]Howden Compressors Ltd., Research and Development,
Glasgow, UK
Contact Information (david.buckney@howden.com)

[2]City University London, Centre for Positive Displacement
Compressor Technology, London, UK

* Corresponding Author

ABSTRACT

A procedure is presented to estimate local clearance distortions in a twin screw compressor using boundary conditions derived from a chamber model. Time varying boundary conditions from the non-dimensional model are mapped onto rotor and casing surface arrays. The fluid boundary temperatures are time-averaged then used to estimate the local rotor and casing temperatures. Heat transfer assumptions that represent the extreme case for component temperature distributions are presented. The relative local change in clearances between rotors and casing are then investigated analytically. The effect of the revised clearances on the performance is quantified and compared against experimental results.

1. INTRODUCTION

Twin screw compressors are positive displacement machines that feature two helically geared rotors. Compression chambers are formed between the close proximity of the rotors with the casing. Clearances are an integral feature of twin screw compressors (see Figure 1) that are necessary to prevent unwanted rotor contact and ensure reliability. These clearances must be carefully managed in order to minimise leakage paths and thermodynamic losses within the compressor. Clearances must accommodate manufacturing and assembly tolerances and operational deformations; the latter consideration is highly dependent on the compression duty and the compression fluid so it is important to match the designed clearances to the application.

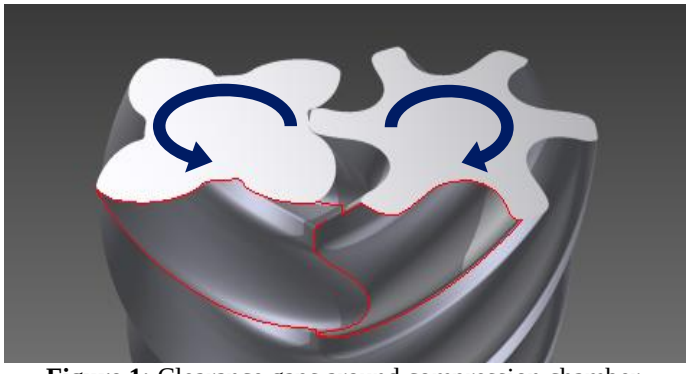

Figure 1: Clearance gaps around compression chamber

The ‘operational clearances’ for a given compressor and compression application are influenced by movements due to pressure forces and bearing clearances and, more significantly in oil free machines, by thermal distortions (Kovacevic *et al.* 2002). Thermal distortions depend on the actual temperature distributions in the rotors and casing as well as the geometry constraints for that compressor. Due to the complex and 3-dimensional nature of this problem a full analysis would require the use of finite difference methods to simulate the local interactions between the solid and fluid domains. An example of a hybrid approach to clearance analysis in the literature uses finite element analysis (FEA) coupled with a lumped analysis of the thermodynamics using a quasi one-dimensional chamber model (Sauls *et al.* 2006).

Quasi one-dimensional chamber models are the industrial standard for design and performance evaluation of screw compressors (Stosic *et al.* 2005). These models efficiently simulate compressor thermodynamic performance by considering a non-dimensional control volume. This control volume varies throughout the compression cycle as a function of the main rotor angle, or cycle angle. At discrete cycle angles the fluid properties within the control volume are calculated; in this way the fluid properties are described throughout the compression process. From this, performance characteristics such as flow and indicated power are easily derived without the need to model actual 3-dimensional flow domains. These models generally assume rigid compressor elements when evaluating leakage areas. In order to predict the influence of thermal clearance deformations iterative corrections can be applied to the defined clearances. Clearance corrections can be based on FEA as mentioned previously or by using either empirical or approximate corrections related to the operating temperature (Buckney *et al.* 2013).

In this paper, a novel procedure is presented to estimate local clearance distortions by applying boundary conditions derived from a quasi 1-dimensional chamber model. Time varying boundary conditions from the non-dimensional model are mapped onto rotor and casing surface arrays. The fluid boundary temperatures are time-averaged then used to estimate the local rotor and casing temperatures. Heat transfer assumptions that represent the extreme case for component temperature distributions are presented. The relative local change in clearances between rotors and casing can then be estimated without the need for FEA. Revised leakage areas which account for thermal distortions are fed back into the chamber model to provide improved performance predictions. The accuracy of the corrected predictions is assessed using test results from an oil free compressor.

2. FLUID BOUNDARY CONDITIONS

2.1 Boundary Surface Arrays

The internal compressor geometry is broken down into a number of discrete surfaces that are exposed to the compression chamber. These surfaces are: casing inlet plane, casing outlet plane, casing bore and rotor section (ridge or flute). Each of these surfaces is repeated for the main rotor and gate rotor sides of the compressor resulting in a total of eight surfaces. Using simple, discrete surfaces it is straightforward to define any location on the individual surface using a 2D array. The surface definition of the main rotor will be presented as an example.

The 3-dimensional surface of the rotor (see Figure 2) is derived using the transverse rotor co-ordinates. Any given point on the rotor surface is defined using a cylindrical co-ordinate system where the rotor radius and the axial position are both constant. The angular position of a fixed point on the rotor varies as a function of the cycle angle.

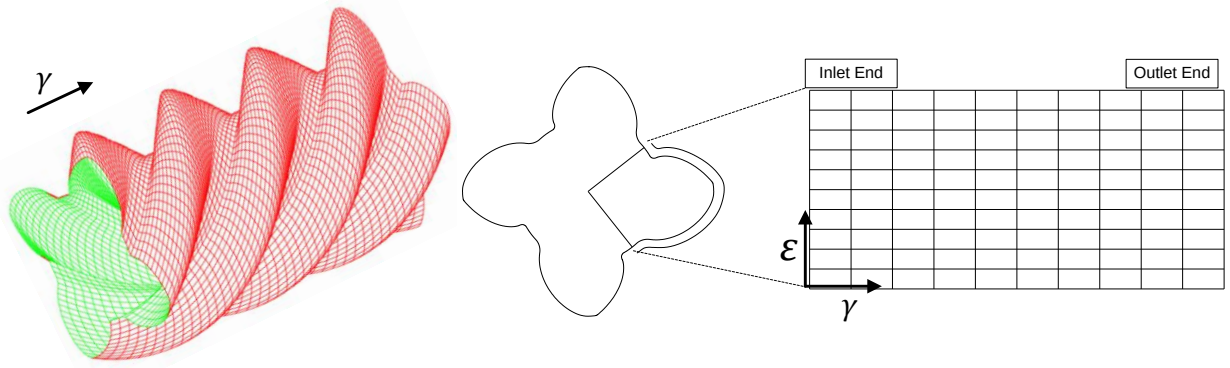

Figure 2: Surface array for main rotor

Assuming steady state operation, the same compression process will repeat in each working chamber and therefore only one rotor 'ridge' or 'flute' needs to be considered. A single rotor ridge is identified on the transverse section of the rotor profile shown in Figure 2. The relative position along the length of the highlighted rotor ridge is defined by the parameter epsilon, ε, which varies: $0 \leq \varepsilon \leq 1$. The second parameter gamma, γ, describes the location along the axial length of the rotor. Local interactions between coincident surfaces will later be investigated using properties assigned to individual points on the relevant surface arrays.

2.2 Mapping Fluid Properties

The fluid properties calculated by a chamber model vary only with the cycle angle; so the key to understanding the local boundary conditions at any compression surface is to calculate what portion of the compression cycle any given point sees. For a point on the casing the 'local' cycle repeats for every passing lobe of the compressor rotors as presented by Sauls *et al.* (2006). For a point on the rotors, the local cycle repeats for every full rotation of that rotor. The boundaries that distinguish the different compression chambers on the rotors are defined by both the radial (rotor to casing) and interlobe (rotor to rotor) sealing lines. Figure 3 shows a transverse cross section of a pair of meshing rotors in which the chamber boundaries can be observed as sealing points. Along the main profile ridge highlighted by line AB, the location of three rotor to rotor (interlobe) chamber boundaries are identified. The highlighted ridge is therefore exposed to four separate compression chambers.

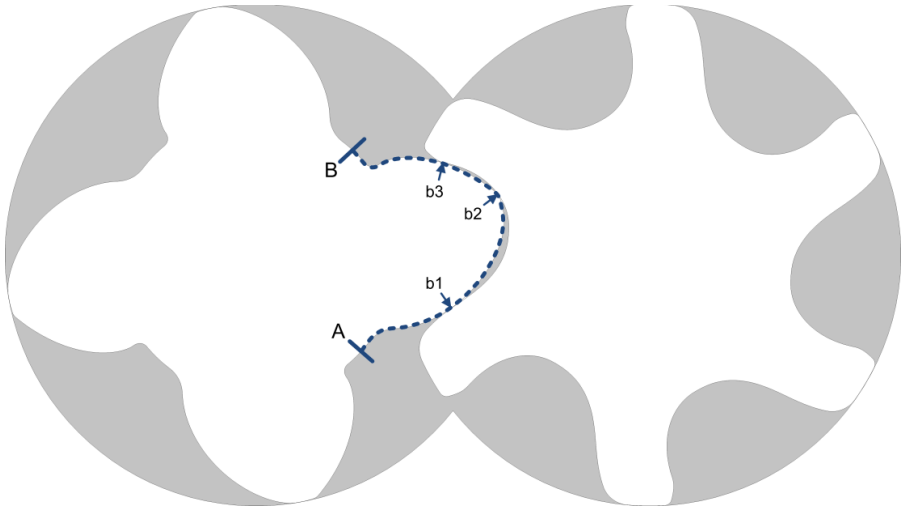

Figure 3: Identifying chamber boundaries on main rotor

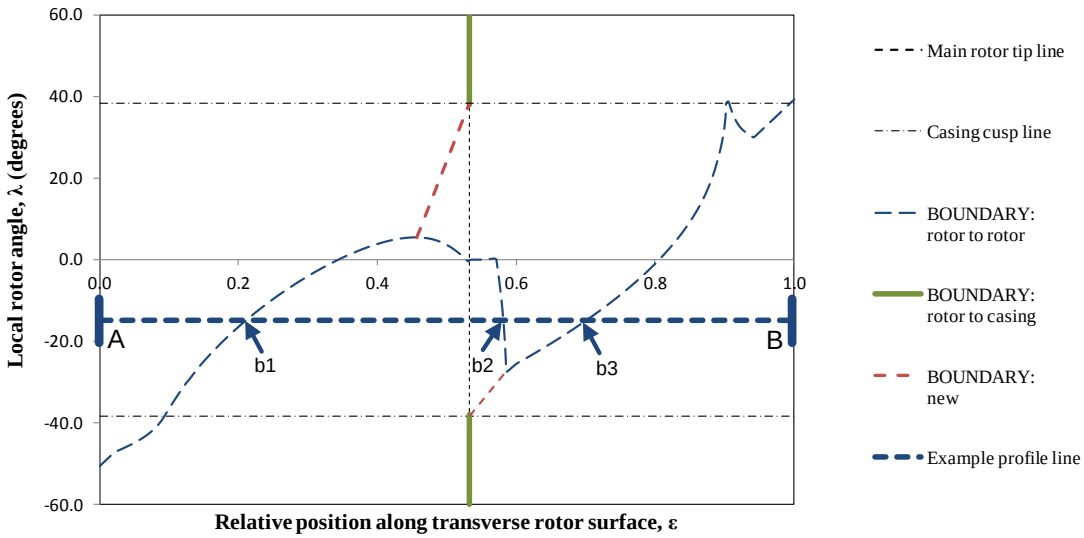

Figure 4: Map of main rotor boundaries

A general method to define the rotor chamber boundaries has been devised; some details of which are presented in Figure 4. The vertical axis describes the angular position of the transverse rotor profile shown in Figure 3 – this has been defined as the local rotor angle, λ, which will vary as a function of the compressor cycle angle and the axial position along the length of the helical rotors. This is plotted against the rotor surface parameter epsilon, providing a way to create a general representation of all rotor surface boundaries.

The top and the bottom of Figure 4 is separated by the interlobe sealing boundary and the left and the right side are separated by the radial sealing boundary, this creates 4 distinct chamber quadrants. In reality the radial boundary does not meet up with the interlobe boundary causing a discontinuity - this is the location of the blow-hole leakage path. New boundaries have been introduced along a straight line in order to distinguish where one chamber ends and the other begins along the path of the blow-hole.

In order to illustrate how this chart works, the transverse rotor ridge along line AB that was highlighted in Figure 3 has been included in Figure 4 – both show the same interlobe boundary points. The local compressor cycle angle in any given chamber quadrant is easily derived for a reference rotor position by applying relevant offsets. There are 360° between the top and bottom quadrants (separated by the interlobe boundary) and 360°/z1 between the left and right quadrants (separated by the radial boundary).

Once the local compression cycle angle is known at each location on the rotor surface array, homogeneous fluid properties from a chamber model can be assigned. In Figure 5a, the instantaneous temperature distribution from the main rotor surface array has been used to build a 3D representation of the full rotor. In Figure 5b the rotor boundary temperature at each local point on the rotor surface has been averaged over one full rotation of the rotor – this represents the time-averaged fluid temperature distribution at the rotor surface.

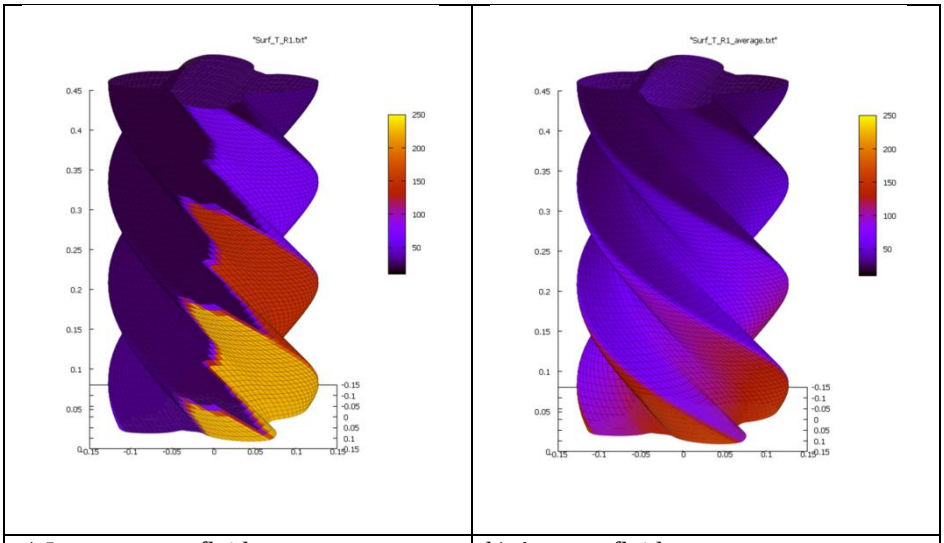

a) Instantaneous fluid temperature | b) Average fluid temperature

Figure 5: Rotor boundary temperature

3. ROTOR AND CASING THERMAL ANALYSIS

The fluid boundary conditions presented in Figure 5 can be similarly calculated for all compressor surfaces exposed to the compression chamber. These boundary conditions can be used for thermal analysis of the compressor rotors and casing. Component temperature distribution depends on: temperature at all fluid boundaries; local heat transfer coefficients; conduction within fixed components; radiation between components and to surroundings. Then, thermal distortions are further affected by stresses introduced due to: thermal gradients; and physical constraints on components. The realism of the thermal analysis depends on accurate and full representation of the compressor geometry as well as the selection of realistic boundary conditions describing how the compressor interacts with the surrounding environment and connected systems. This generally requires the use of a numerical finite difference method which represents the full component geometry and constraints.

For the purposes of assessing how thermal distortions affect local clearances and performance at a conceptual design stage, significant simplifying assumptions must be made. This approach does not attempt to provide maximum realism for a particular case but rather provide a general approximation of rotor thermal behaviour. An objective in this work to quantify local clearance variations is to assess reliability therefore the assumptions below aim to represent extreme cases for thermal distortions.

3.1 Heat Transfer Assumptions

Conduction along the axial length of the rotors is neglected. This means there is no heat transfer from the hot end to the cold end of the rotor and no heat transfer along the rotor shafts to or from the bearings. This results in a local maximum rotor temperature which is probably higher than the actual maximum.

It is assumed that the heat conduction across the transverse section of the rotors dominates over convective heat transfer at the rotor surface. This allows the time-averaged local fluid boundary temperatures shown in Figure 5b to be averaged across the full transverse rotor section. The estimated rotor temperature therefore only varies along the rotor length as shown in figure Figure 6a.

The casing geometry is simply represented by the internal surface as in Figure 6b, which shows the casing bore surfaces. It is assumed that no conduction occurs in any direction across this surface and that there is no heat transfer to the surroundings. This again results in a local maximum casing temperature that is probably higher than the actual maximum. With this assumption the local casing temperature can be approximated as the time-averaged fluid boundary temperature.

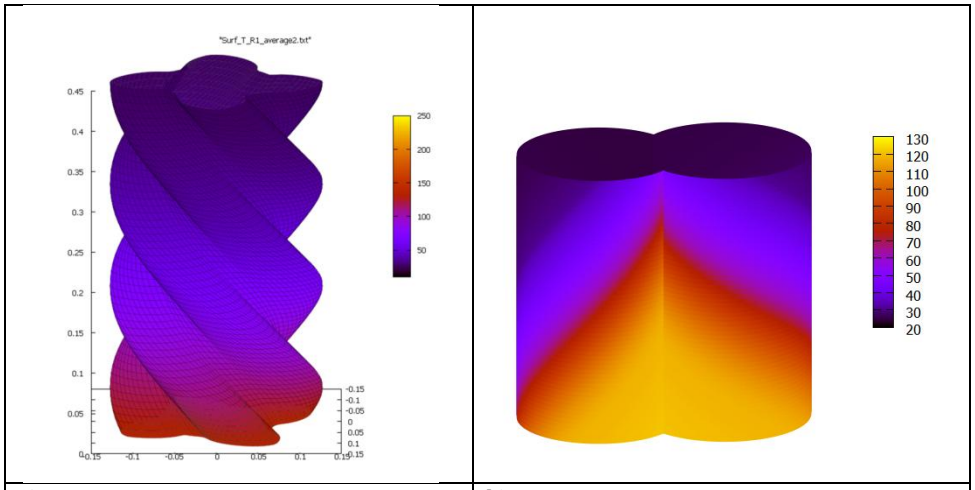

a) Rotor temperature | b) Casing temperature

Figure 6: Assumed rotor and casing temperature distributions

3.2 Approximating Thermal Distortions

Local displacements have been calculated using analytical approximations. The change in the local interlobe gap is calculated using a 2-dimensional approach that is repeated at each transverse location along the length of the rotors. Figure 7 shows the known location of a local sealing point under investigation. Thermal distortions are evaluated analytically for: main rotor dimensions x_1 and y_1; gate rotor dimensions x_2 and y_2; and the casing dimension A (interpolated between thermal growth at suction and discharge faces).

The close up of the intelobe gap in Figure 7 shows the transverse clearance gap, G_{IT}, and it's components, G_{Ix} and G_{Iy}. The change in the gap is related to changes in the rotor and casing dimensions as described in equations 1 and 2. Equation 3 states approximations that allow further simplification of the analysis by eliminating the need to use the gate rotor dimensions. Once known, the *transverse* gap can be used to determine the *normal* gap (Holmes, 1990)

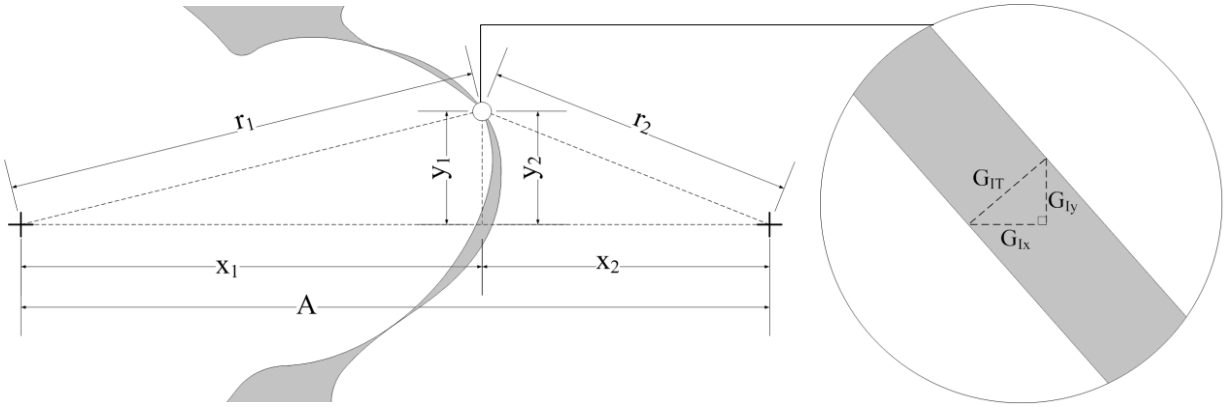

Figure 7: Local definition of intelobe gap

$$\Delta G_{Ix} = -\Delta x_1 - \Delta x_2 + \Delta A \tag{1}$$

$$\Delta G_{Iy} = \left(\frac{(x_1 - r_{1w})}{|(x_1 - r_{1w})|}\right)(|\Delta y_2| - |\Delta y_1|) \tag{2}$$

$$x_2 \sim (A + x_1); \quad y_2 \sim y_1 \tag{3}$$

In the case of the local radial gap a 1-dimensional analytical approach was taken. The main rotor axis and main rotor casing bore axis are taken as a common datum for thermal growth of that rotor and casing bore (similarly for gate rotor side). Component stresses due the thermal gradients and constraints are neglected and casing thermal distortions are based solely on the local temperature and the reference distance to the common datum.

4. CASE STUDY

The following study was undertaken to assess how clearances are affected by local thermal distortions and, by feeding results back into the thermodynamic chamber model, to determine what impact this has on the compressor performance. The proposed clearance corrections were applied for a 3/5 lobe, oil free compressor with main rotor diameter of 128mm and length to diameter ratio of 1.6. The compressor was run with atmospheric air at suction. Due to the lack of compressor cooling and the high adiabatic exponent of air, the achievable pressure ratio is restricted by the operating temperature and the impact this has on operating clearances. Performance test results for such a compressor will be compared with the model predications. The following model cases will be used to investigate the sensitivity of the interlobe clearance to the proposed rotor and casing thermal corrections:

Table 1: Modelled cases

Clearance Adjustments	**Case A**	**Case B**	**Case C**
ROTOR thermal distortion	No	Yes	Yes
CASING thermal distortion	No	No	Yes

4.1 Clearance Sensitivity

In Figure 8 the local interlobe clearance gap is plotted against s - the relative position along the interlobe sealing line for a single compression chamber. This sealing line follows the 3-dimensional rotor to rotor boundary which is best visualised in Figure 1. In Figure 8 the location of the rotor root and tip is annotated and the local rotor radius is plotted on the secondary axis to provide an indication of the local clearance positions.

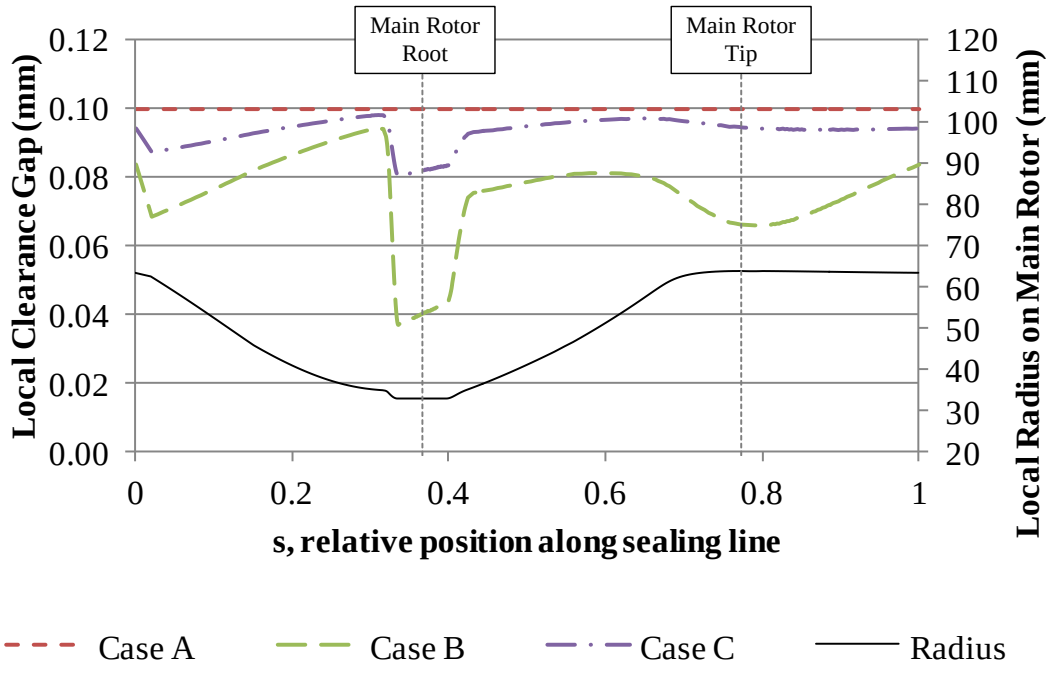

Figure 8: Interlobe clearance distribution corrected for thermal deformations

In Case A no corrections have been applied and the local clearance gap has been taken to be a constant value of 0.1mm. With the introduction of the rotor thermal expansion in Case B we can see significant clearance reduction with some local areas more affected than others. The location of the biggest clearance reduction is at the root of the main rotor suggesting that this is where rotor contact is most likely to occur. The thermal expansion of the casing in Case C mitigates the rotor expansion as would be expected however there is still a slight net decrease in the interlobe clearances for this case.

The results shown in Figure 8 are for a specific instant in the compression cycle when the interlobe sealing line is fully developed. The instantaneous interlobe leakage area is taken as the area under the relevant curve (corrected for the actual sealing line length). As the cycle progresses, the length and position of the sealing lines change and the local clearance deformations need to re-evaluated based on the new location. Figure 9 shows the changing history of two leakage areas beginning at the start of compression (in this case when $\theta = 0°$). The left hand of Figure 9 is the interlobe leakage area curve (this is related to the clearance distribution of Figure 8). The right hand of the figure is the combined leakage area curve for all out-flow radial clearances. It is interesting to note that for Case C, with rotor and casing expansion, a net increase in the radial gap is predicted in the latter stages of the compression cycle due to the local hot spot on the compressor casing. The radial leakage area is greater than the interlobe leakage area. What is not show in this paper is that a similar radial in-flow leakage area will also exist that feeds some mass flow back into the rotor chamber from the previous chamber. The pressure difference across the radial leakage area is significantly smaller than across the interlobe gap which skews the relative significance of these flow areas to the thermodynamic performance.

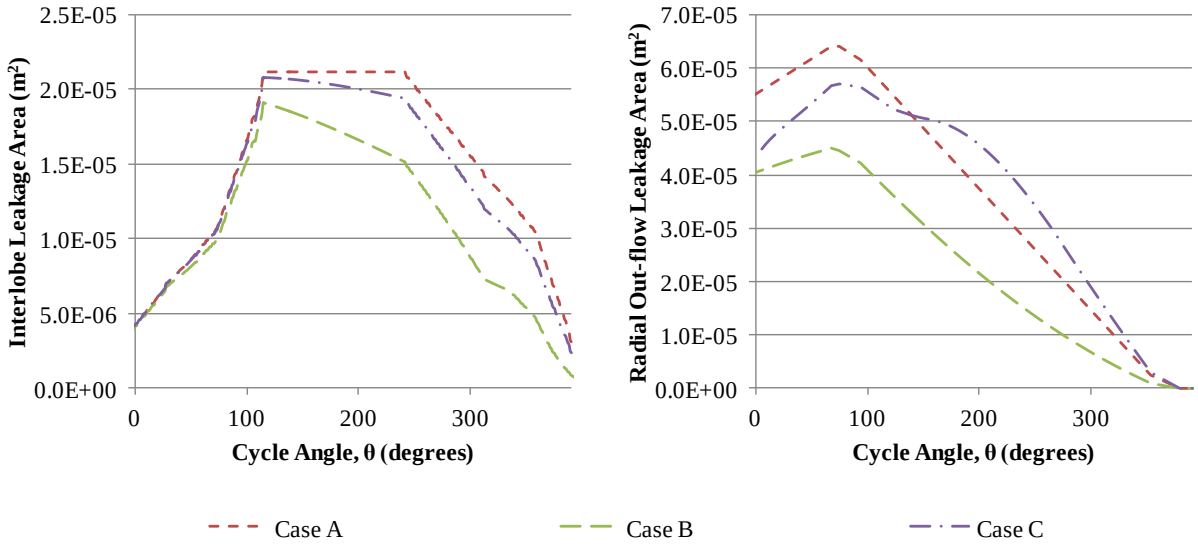

Figure 9: Variation of leakage areas throughout compression cycle

4.2 Performance Results

In Figure 10, measured tests results of compressor flow and discharge temperature have been used as a benchmark to compare model predictions. During modelling, initial boundary conditions are based on results from a chamber model with no clearance corrections (as in Case A), thereafter some iteration is required until clearance corrections and thermodynamic results stabilise (for Case B and C).

The results of the model running Case B - with interlobe and radial clearances corrected for rotor thermal growth only - show a significant increase in flow compared to the results of Case A. Case B also has a smaller drop off in flow with increased pressure ratios (flatter gradient in trend) that is closer to the measured gradient than Case A. The results of the model running Case C - with interlobe and radial clearances corrected for rotor and casing thermal growth - show an improvement in the absolute flow values however there is a deviation from the measured gradient. The right hand side of Figure 10 shows that the modelled temperature is closer to the measured results in terms of absolute values and gradient (with respect to pressure ratio) for both cases with clearance corrections.

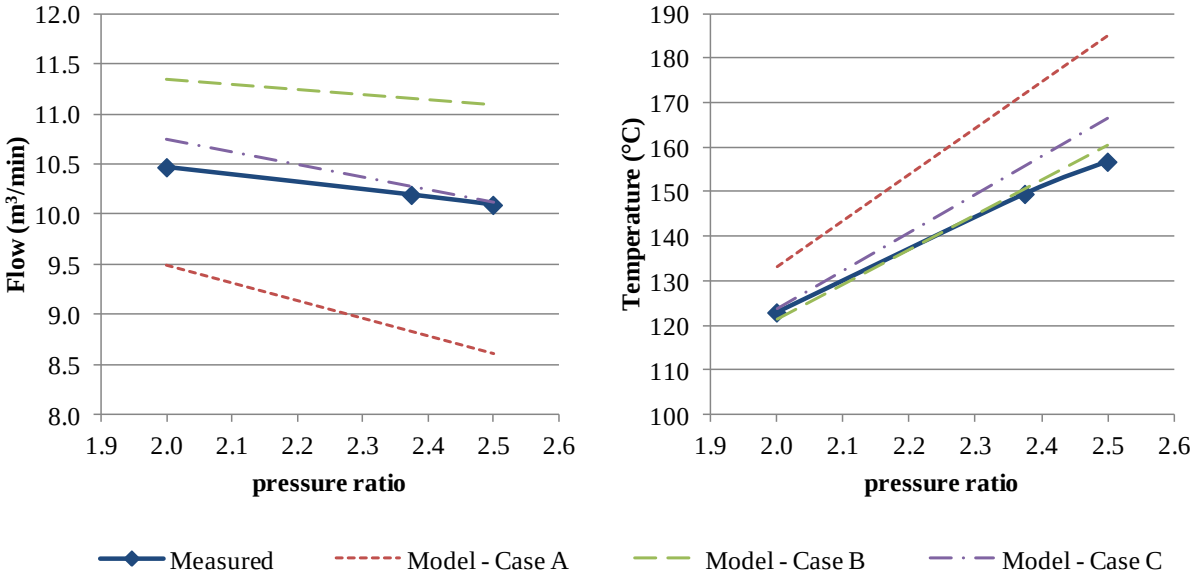

Figure 10: Compressor performance from test and model

5. CONCLUSIONS

A procedure has been presented to map thermodynamic results from a lumped parameter chamber model onto discrete surface arrays. This provides useful boundary conditions for further thermal analysis of compressor components.

Surface boundary conditions were used to estimate the temperature distribution of the compressor rotors and casing that result in the largest feasible peak temperatures during normal operation. When possible, it is planned to validate these temperature distributions with results from FEA and test measurements.

Local variations in clearances, due to thermal distortions, have been approximated analytically. This provides valuable data at an early design stage about where and when in the compression process clearances are not adequate for a given compression application. Integrating this information into the rotor design process allows a more optimised balance between reliability and compressor performance.

Revised performance prediction using updated leakage areas shows the modelled flow and discharge temperature to be very sensitive to operational clearance variations. In the case study presented, model accuracy improved with the introduction of local clearance corrections used to iteratively calculate leakage areas.

There is an inherent degree of uncertainty in the approximated clearance corrections, particularly in the casing thermal corrections, that are estimated without representing the full compressor geometry. This uncertainty is compounded by the fact that the actual assembled clearances of the compressor are subject to rotor profile and lead tolerances as well as stacked assembly tolerances. These are factors that will always have a bearing on the absolute value of performance predictions (and for that matter on the repeatability of test results from different compressors of the same type). Nonetheless, this has shown to be is a useful tool that can be applied as part of a broader approach to improve accuracy of twin screw compressor chamber models.

NOMENCLATURE

A	start point, rotor centre distance
B	end point
G	clearance gap
b	boundary point

r	radial dimension
s	relative position along interlobe sealing line
x	dimension
y	dimension
z	number of lobes on rotor
θ	cycle angle
λ	local rotor angle
ε	relative position along transverse rotor profile

Subscript

1	main rotor
2	gate rotor
T	transverse
x	x component
y	y component

REFERENCES

Buckney, D., Kovacevic, A., Stosic, N., 2013, Experimental Validation of a Geometry Model for Twin Screw Machines, *IMechE International Conference on Compressors and their Systems*, London.

Holme, C.S., 1990, *A Study of Screw Compressor Rotor Geometry Leading to a Method for Inter-Lobe Clearance Measurement*, Doctoral Thesis, Huddersfield Polytechnic.

Kovacevic, A., Stosic, N., Smith, I., 2002, The influence or rotor deflection upon screw compressor performance. *VDI BERICHTE*.

Sauls, J., Powell, G., Weathers, B., 2006, Transient Thermal Analysis of Screw Compressors, Part I Use of Thermodynamic Simulation to Determine Boundary Conditions for Finite Element Analyses, *International Engineering Compressor Conference at Purdue*.

Stosic, N., Smith, I., Kovacevic, A., 2005, *Screw Compressors, Mathematical Modelling and Performance Calculation*, Springer.

ACKNOWLEDGEMENT

The authors would like to thank Howden Compressors Ltd. for supporting this research and City University for their collaboration and access to experimental results.